Computer simulations reveal motor properties generating stable antiparallel microtubule interactions

François Nédélec

Cell Biology and Biophysics Program, European Molecular Biology Laboratory, 69117 Heidelberg, Germany

An aster of microtubules is a set of flexible polar filaments with dynamic plus ends that irradiate from a common location at which the minus ends of the filaments are found. Processive soluble oligomeric motor complexes can bind simultaneously to two microtubules, and thus exert forces between two asters. Using computer simulations, I have explored systematically the possible steady-state regimes reached by two asters under the action of various kinds of oligomeric motors. As expected, motor complexes can induce the asters to fuse, for example when the complexes consist only of minus end–directed motors, or to fully separate, when the motors are plus end directed. More surprisingly, complexes made of two motors of opposite directionalities can also lead to antiparallel interactions between overlapping microtubules that are stable and sustained, like those seen in mitotic spindle structures. This suggests that such heterocomplexes could have a significant biological role, if they exist in the cell.

Introduction

In eukaryotic cells, polar filaments and associated proteins play an essential role in determining intracellular order. Microtubules are often found in highly connected structures, such as the mitotic spindle in dividing cells (Karsenti and Vernos, 2001; Wittmann et al., 2001) or complex arrays in differentiated cells. These cellular assemblies can be observed and perturbed, and this has yielded invaluable insights into their modes of organization and their dynamic properties. Microtubules can be reconstituted from pure tubulin, with the optional addition of other purified cytoskeletal proteins, and these in vitro studies have provided quantitative data about their physical properties. However, although the filaments, many associated proteins, and most of the molecular motors participating in the spindle have been identified, and much is known about their individual modes of action, we still understand poorly how they participate collectively to the morphogenesis and steady-state dynamics of this structure. Questions as to how a balance of forces is achieved and what makes it stable are difficult to address in quantitative terms in real spindles. It seems that to examine such fundamental questions, it is desirable to study structures with intermediate levels of complexity and to develop tools to handle them.

Computer simulations are one such tool, and they have been used before to examine the motility of polar filaments driven by immobilized motors (Bourdieu et al., 1995; Gibbons et al., 2001), microtubule dynamic instability (Bayley et al., 1989; Gliksman et al., 1993; Dogterom et al., 1995), actin bundle contraction (Nakazawa and Sekimoto, 1996; Kruse and Julicher, 2000), aster centering inside a box (Holy et al., 1997), and the formation of microtubule asters by soluble oligomeric motors (Nédélec et al., 1997, 2001; Surrey et al., 2001).

Here I describe computer simulations that calculate the evolution of a set of dynamic filaments with motor proteins. Using these stochastic simulations, I examine how two asters of dynamic microtubules nucleated by two microtubule organizing centers can reach a steady-state configuration in which microtubules overlap fully or partially. Such overlaps are essential in some spindles to counteract the forces that pull the chromosomes apart.

Results

To investigate theoretically whether bifunctional motors can produce a stable interaction between two microtubule asters, a simulation was built (see Materials and methods). It includes asters composed of a variable number of dynamic and flexible microtubules, and oligomeric motor complexes that can bind up to two microtubules, ultimately producing forces between the asters.

Although the situation studied is very simple compared with that in a cell, its quantitative description already required ~27 parameters (Table I), and the first problem was to find values for all of them. Three parameters are model specific and do not reflect any real property (e.g., the time step dt);

Address correspondence to François Nédélec, Cell Biology and Biophysics Program, European Molecular Biology Laboratory, Meyerhofstrasse 1, 69117 Heidelberg, Germany. Tel.: 49-6221-387-360. Fax: 49-6221-387-512. E-mail: nedelec@embl-heidelberg.de

Key words: spindle; cytoskeleton; molecular motor; aster; model

Table I. **Parameters of the simulation**

Parameter description	Symbol	Value or range of values
Model-specific parameters		
Time step	dt	10^{-2} s
Filament section	R	1.2 μm
Simulation box		square, 60 × 60 μm
Fixed parameters		
Total simulated time		1,000 s
Temperature	k_BT	4.2×10^{-3} pN μm
Fluid viscosity	viscosity	0.05 pN s/μm^2
Microtubule's bending modulus	E	20 pN μm^2
Microtubule dynamic instability: catastrophe and rescue frequencies		rescue in s^{-1}, (13 − L) × 0.0033; catastrophe in s^{-1}, L × 0.003[a]
Growth and shrinking speeds		+10 and −15 μm/s
Complexes diffusion	D	20 μm^2/s
Independently varied parameters		
Number of microtubules per aster		between 20 and 80, same for both asters
Motor links rigidity	K	between 5 and 60 pN/μm
Number of complexes: one parameter in screens 3a, b, and c, and two parameters in screens 1 and 2		between 500 and 15,000
Motor's speed (2 parameters)	V_{max}	between −1 and +1 μm/s[b]
Motor's stalling force (2)	F_{max}	between 0.5 and 2 pN, with $F_{max}^2 > 9.dim.K.k_BT$
Motor's binding rate (2)	P_{on}	between 0.04 and 50 s^{-1}
Motor's unbinding rate (2)	P_{off}	between 0.04 and 50 s^{-1}
Motor's unbinding rate from microtubule end	P_{end}	$P_{end} > 100$ s^{-1} in screens 1, 2, and 3a, and 0.04 to 50 s^{-1} in screens 3b and c
Motor's force–velocity type (2)		one of four models (see Materials and methods)
Derived parameters		
Motor's reach distance	ϵ	equals F_{max}/K (see Materials and methods)

[a]L, length of microtubule in μm.
[b]V_{max} is rounded to a multiple of 0.01 and $V_{max} = 0$ is excluded.

their values were chosen to generate sufficient numerical precision (see Materials and methods). Many of the other parameters describe known properties of the situation studied, i.e., temperature, viscosity of the fluid, microtubule rigidity, and dynamic instability, and were set accordingly. What remained unspecified were the number of microtubules in each aster and the parameters describing the motors.

There are estimates for the values that would be appropriate for conventional kinesin, and they have been successfully used to simulate the behavior of synthetic kinesin complexes in in vitro experiments (Nédélec et al., 2001, Surrey et al., 2001). However, the motors involved in spindle organization have not yet been thoroughly biophysically characterized. Most of their in vivo characteristics, i.e., force, speed, processivity, are still unknown. To avoid an arbitrary choice, a different approach was chosen, where these parameters were set randomly within a reasonable range (Table I). Thus to probe the generic possibilities of the system, parameter sets were generated to represent a possible number of microtubules and combinations of motor characteristics: many or few, plus or minus directed, fast or slow, strong or weak, and high or low rates.

In essence, I performed a virtual screen for possible steady-states for the relative position of two asters exposed to various motor complexes. The screen was based on the automatic selection of "persisting interactions" between two asters among a collection of simulations generated automatically, with "interaction" meaning that the two asters are linked by motor complexes. Specifically, for each generated parameter set, a simulation was started from unbound motors and two randomly positioned asters, and the evolution in time was calculated for 1,000 s of simulated time. A total of ∼50,000 simulations in one dimension (1D)* and ∼10,000 simulations in two dimensions (2D) were computed. From these, interactions that persisted in time were selected, and unstable or transient patterns discarded by an automatic scan that retained only those simulations that had always at least one motor complex linking the two asters together, after an initial 500 s, which allowed the system to equilibrate. The selected simulations fell in one of only four categories: fusion, separation of the asters, oscillations of the asters, or stable antiparallel interactions.

Overall, 40% of the simulations were persisting interactions. From the correlations in the corresponding parameters, it was found for example that low off-rate compensates for low on-rate, or high motor concentration compensates for low on-rate (unpublished data). Most of these correlations simply show that the motors must have a certain "efficiency" to produce a persisting interaction: the rates and concentrations should define an equilibrium in which sufficient motors can bind two microtubules that are crossing or overlapping. This is a basic requirement that does not by itself guarantee success. Motors with inappropriate speeds, however efficient they are, never lead to persisting interactions.

Five screens have been performed (Fig. 1) in which two different motors, u and v, were simulated. By convention, u and v will also designate the speeds of these motors, with positive values for plus end–directed motors and negative

*Abbreviations used in this paper: 1D, one dimension; 2D, two dimensions; 3D, three dimensions.

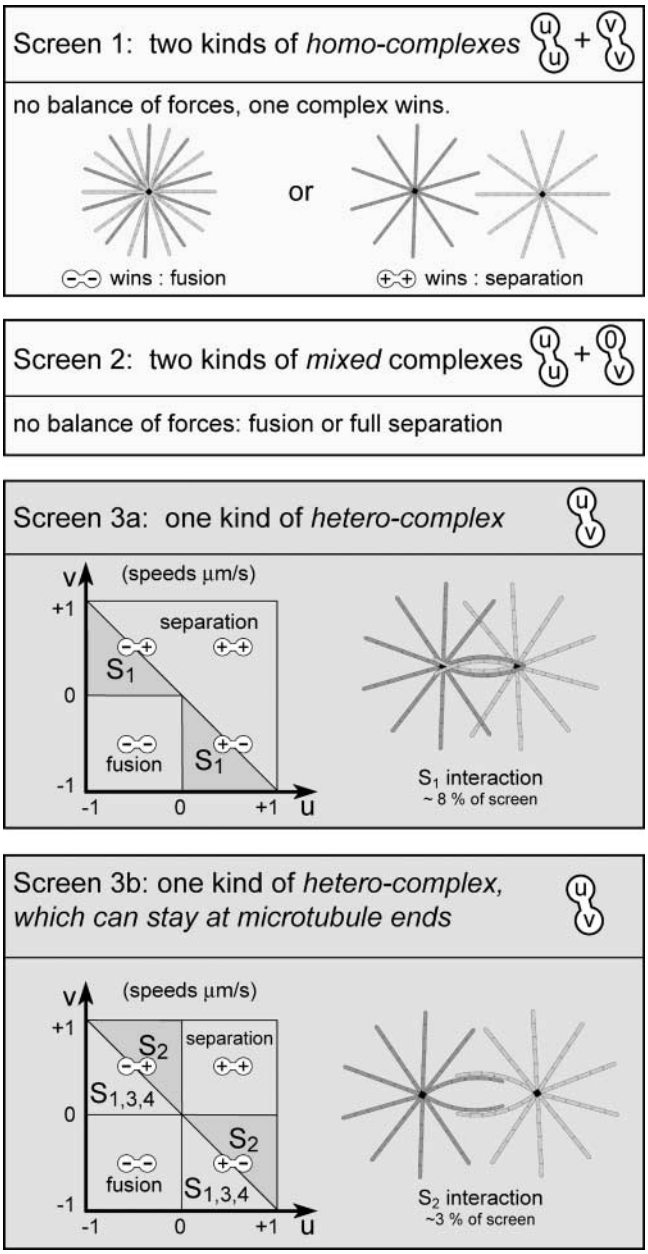

Figure 1. **Summary of the screens.** Screen 1 was performed with two kinds of homocomplexes, with all sorts of configurations of minus or plus end–directed motors. It produced fusion of the asters or their full separation. Screen 2 is inspired by the putative configuration of the biological motors involved in the spindle. Screen 3a was performed with one kind of heterocomplex. It produced fusion, full separation, oscillations, and one type of nonfused stable interaction, solution S_1. To achieve S_1, the speeds of the motors u and v need to satisfy $u + v < 0$ and $u \times v < 0$, as depicted in the diagram. Screen 3b is a variation in which the motors could hold on to the microtubule ends. Four solutions are found, as discussed in the text.

values for minus end–directed motors. The screens differed in the way that the motors were assembled into complexes. Screen 1 considered two kinds of homomotor complexes, i.e., schematically u–u and v–v. Screen 2 considered homomotor complex u–u and MAP motor complex v–z, with z, a motor of speed zero, in the model. Screens 3a, 3b, and 3c considered one kind of heteromotor complex (u–v). In all these screens, the number of parameters varied (Table I) and the number of simulations (~2,000) calculated were similar.

Screen 1

With two sorts of homocomplexes (u–u and v–v) in all the combinations of directionality, speed, forces, and rates, all persisting interactions resulted in the fusion or the full separation of the two asters. This was usually achieved within 1,000 s, but in rare cases of slow dynamics, the simulations had to be prolonged in time to reach fusion or full separation. A persisting interaction with a nonzero distance between the centers was not found. With only minus end–directed motors, the fused configuration was globally stable. In the presence of homocomplexes of plus end–directed motors only, the fused situation was stable or metastable, but only arose if the asters were initially very close. When the asters were initially far enough apart, they separated further under the action of motors binding antiparallel microtubules (see Fig. 4).

Screen 2

The next screen was inspired by a proposed model of the mitotic spindle, in which the motors Eg5 and Ncd balance their forces to determine the overlap zone (Sharp et al., 1999). Eg5 is a homotetramer and has been proposed to cross-link two microtubules (Kashina et al., 1996), behaving essentially like a slow (in vitro, ~0.03 µm/s) double plus end–directed complex. Ncd has a minus end–directed motor domain in its COOH terminus (in vitro, −0.25 µm/s; McDonald et al., 1990), but also an additional nonmotor microtubule binding domain (Karabay and Walker, 1999). Thus Ncd can, in principle, also cross-link microtubules. To explore this scenario, Ncd was modeled as a heterocomplex made from a static microtubule binder and a minus end–directed motor (v–z, with $v < 0$ and $z = 0$). Eg5 was modeled as a bifunctional plus end–directed motor (u–u, with $u > 0$). The speeds and other characteristics of these complexes were varied randomly within the usual ranges (Table I). As in the first screen, persisting interactions only resulted in fusion or full separation of the asters.

Screen 3a

As shown in Fig. 1, when heteromotor complexes (u–v) were simulated, the speeds of the motors simply determined which persisting interactions could appear. (1) If $u < 0$ and $v < 0$, a persisting interaction always resulted in the fusion of the asters. (2) If $u + v > 0$, persisting interaction only caused full separation of the asters, with the exception of the metastable situation of initially fused asters. (3) If $u \times v < 0$ and $u + v < 0$, persisting interactions could be of several kinds. Diverse oscillatory solutions were observed (unpublished data; see http://www.embl-heidelberg.de/ExternalInfo/nedelec/asters), provided that the motors unbound at their maximum force (see Materials and methods). They were not studied further. More interesting were some persisting interactions, characterized by a complete antiparallel microtubule overlap in which the distance between the aster centers was never below 2 µm (Fig. 2). By looking precisely at the motor complexes in all these simulations, one could

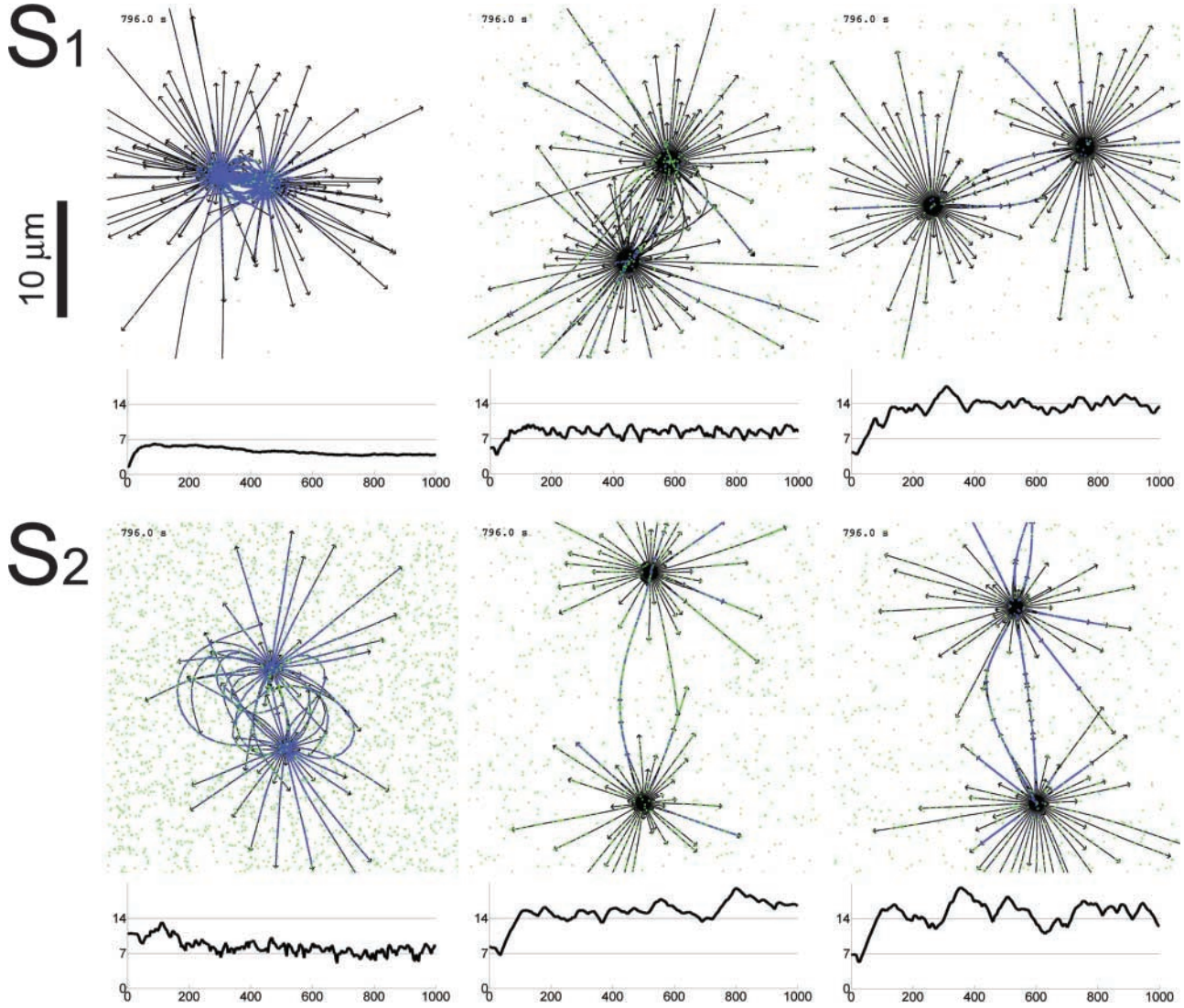

Figure 2. **Examples of stable interactions between dynamic asters with heterocomplexes.** (Top) Solutions of type S_1. The speeds (μm/s) of the two motors forming the complex are as follows: left, 0.35 and -0.91; middle, 0.31 and −0.73; and right, 0.6 and −0.83. (Bottom) Example of solution S_2 speeds are as follows: left, 0.95 and −0.45; middle, 0.47 and −0.45; and right, 0.89 and −0.64. Below each example is plotted the distance between the two asters (μm) as a function of time (s). It is not possible to distinguish from these views the different solutions. See animations at (http://www.embl-heidelberg.de/ExternalInfo/nedelec/asters).

see that the balance of forces was always achieved in the same way. Hence, they all represented the same generic qualitative solution (S_1). S_1 was realized in ∼10% of the simulations in this screen, but the sampling was still too sparse to determine precisely the region in parameter space associated with S_1. However, the speeds of the motors leading to S_1 are found over the entire domain allowed by the two rules $u \times v < 0$ and $u + v < 0$ (see Fig. 6). Other parameters are also important in determining if the motors will produce S_1 or not, but the correlations found are only the ones expected to be needed to produce efficient motors.

The balance of forces defining S_1 can be first described in 1D only, assuming microtubules of equal length. As pictured in Fig. 3, the antiparallel overlap is always total: some microtubules always reach behind the center of the other aster. The attractive force between the asters is mostly produced by motors binding antiparallel microtubules, and the repulsive force is produced by motors bound to parallel microtubules (Fig. 4 A). Both components can be high, typically 100 pN, but cancel each other to produce an equilibrium under tension. The attractive force can be easily understood, as $u + v < 0$ is sufficient for the antiparallel complex configurations to produce attraction (Fig. 4 B). The repulsive forces are more surprising, because one should expect that motors linking two parallel microtubules exert forces that on average cancel each other out (Fig. 4 C). A net force arises only if the two possible configurations (u binds to MT_1 and v binds to MT_2, or v binds to MT_1 and u binds to MT_2) are not equally present. As shown in Fig. 3, this is exactly the case for the motors linking the parallel overlaps in S_1. This asymmetry is a consequence of the movement of motors, which brings them to the overlapping region always in the same configuration.

The equilibrium S_1 is stable. Indeed, the forces are expected to be roughly proportional to the number of doubly

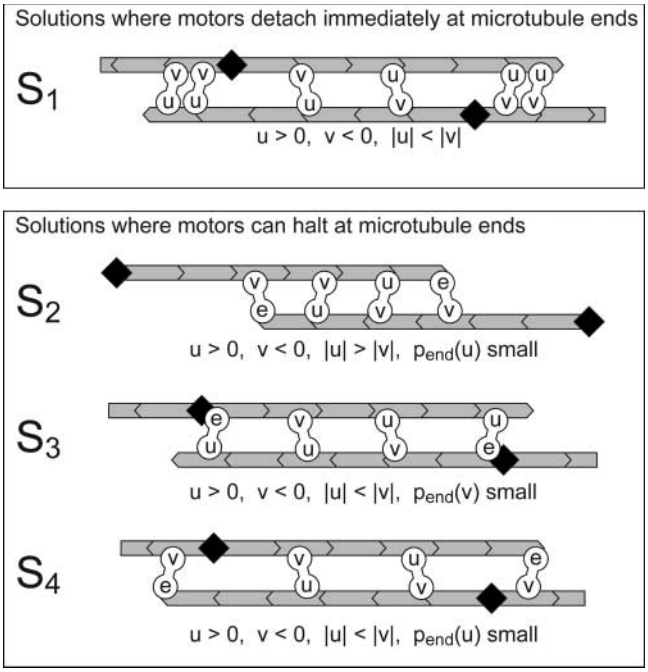

Figure 3. **The balance of forces in the solutions.** Schematic asters in 1D only have two opposing microtubules radiating from a common center represented by a black diamond. All solutions are built from one kind of heterocomplex with two speeds u and v, which must satisfy the conditions specified here. Solution S_1 is found even when motors immediately detach from the end of the microtubules, whereas the others are obtained when the motors can stay at the end (in this situation, u or v is replaced by e). Pushing or pulling is schematically represented here by the tilt of the complex, which is a consequence of the relative movement of both motors. The attractive or repulsive nature of the forces can be deducted by mentally trying to restore the complexes in a vertical position.

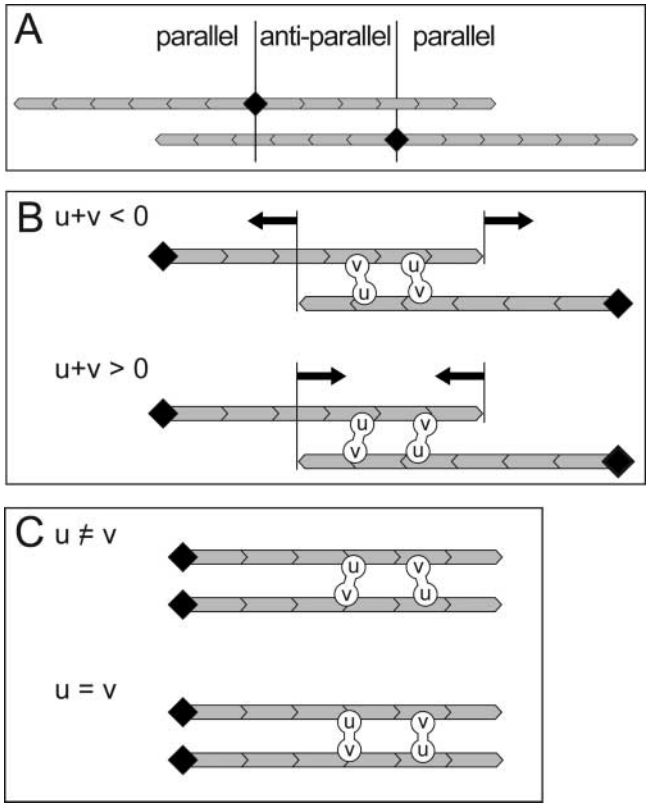

Figure 4. **Symmetry arguments.** (A) Two asters can have antiparallel overlaps, but also parallel ones, when they are close. (B) On an antiparallel overlap, heterocomplexes of speeds u and v produce attractive force if $u + v < 0$, or repulsive force if $u + v > 0$. Both possible motor configurations produce forces in the same direction. (C) On a parallel overlap, if $u \neq v$, the two configurations result in opposite forces. If they are equally probable, these forces cancel each other. A homocomplex ($u = v$) does not produce any force on parallel microtubules and stabilizes the overlap.

bound complexes, which is itself roughly proportional to the length of the overlap (Fig. 3, S_1). So if the asters are pushed apart from the equilibrium position or if microtubules shorten, attractive force will rise and repulsing forces will fall, leading the asters to move back together. The reverse is true if the asters get too close or if microtubules grow. Although the forces are also proportional to the number of complexes in solution, the equilibrium is in fact quite insensitive to the concentration of motors (http://www.embl-heidelberg.de/ExternalInfo/nedelec/asters). This is because both attractive and repulsive forces are produced by the same complexes, only in different configurations. The balance of forces in 2D and 3D (three dimensions) is essentially the same as described in 1D, but there are additional requirements. For example, to sustain equilibrium, the motors need to bend the microtubules that extend off axis, and continuously bring them to overlap with microtubules from the other aster. The microtubule rigidity should also be able to sustain their longitudinal load. The simulations show that all the necessary requirements are indeed met.

To test the uniqueness and accessibility of the equilibrium position, the simulations leading to S_1 were repeated, keeping the same parameters, but starting from different initial configurations and using different random number sequences. The average reliability was high (9 reruns failed out of 227), and many individual S_1 solutions had very high reliability. For example, Fig. 5 shows a simulation in which 100 repetitions never failed to produce the same interaction. All this suggests that S_1 determines a unique equilibrium position that can be reached from any connected initial configuration.

Screen 3b

The screens described so far considered motors that would detach immediately when they reached the ends of their track (high P_{ends}). However, in reality a motor can halt for a short interval when it reaches the end of a microtubule. Therefore, the heterocomplex screen 3a was repeated, this time allowing the motors to stay at the ends of growing microtubules for variable periods of time ($P_{end} = P_{end\_growing}$ varied between 0.04 and 50 s^{-1}), but not at the ends of shrinking microtubules ($P_{end\_shrinking}$ is fast). Three new classes of interactions were found, with antiparallel microtubule overlaps: S_2, S_3, and S_4 (Fig. 3). The first one, S_2, which represented ~3% of the simulations, is particularly interesting, because it was the only one that led to a partial antiparallel microtubule overlap (Fig. 3).

In S_2, the balance of forces is between motors that have reached the end of a microtubule and motors that have not,

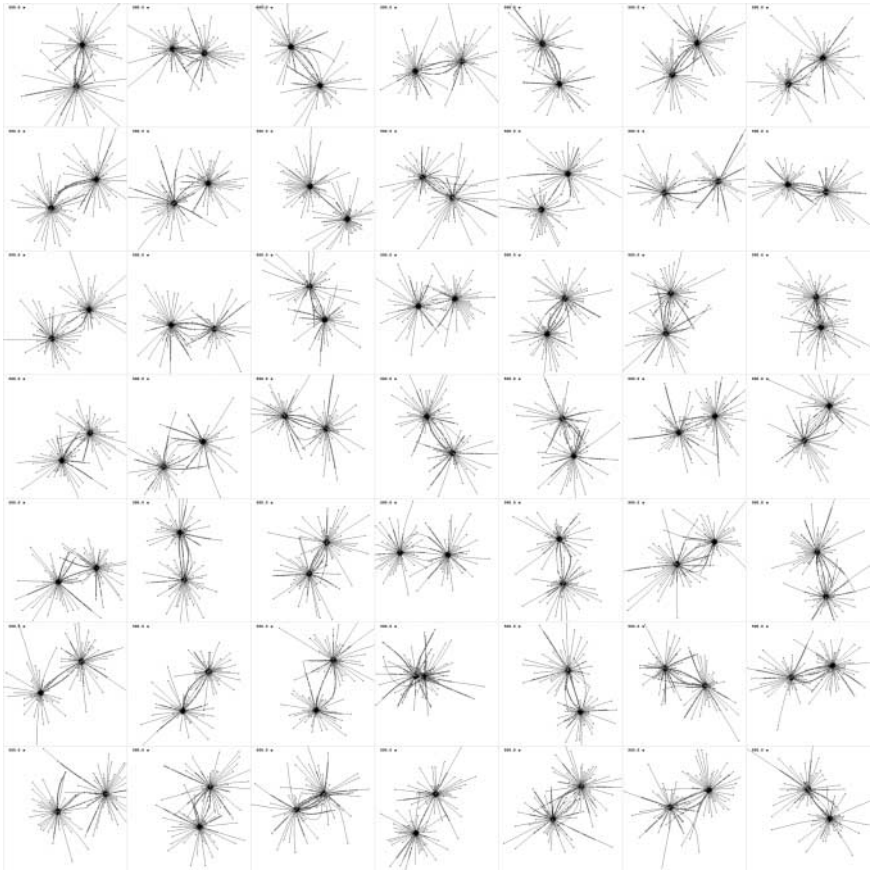

Figure 5. **Reliability of a solution S_1.** Figures produced by 49 simulations, all performed with the same parameter set, but with different initial configurations and random number sequences. The figures are all similar, showing the reliability in which the parameter set determines the evolution of the system toward a unique interaction configuration. Each picture covers 30 × 30 μm.

both acting on antiparallel overlaps (Fig. 3). Hence, the pushing forces are produced by a population of motors whose number is roughly proportional to the length of microtubule overlap, and pulling forces are produced by a population of motors that is proportional to the number of microtubule ends, i.e., more or less constant. Because pushing forces decrease directly with aster–aster distance, whereas pulling forces do not, the asters will be dragged closer or further away until they find a distance at which equilibrium is reached, and this equilibrium will be stable.

A plot shows the requirements on the motor speeds (Fig. 6). S_2 only covers part of the domain $u \times v < 0$ and $u + v > 0$. Motors slower than ~0.25 μm/s seem to be unable to achieve S_2 equilibrium. Simulations with static microtubules produced S_2 with speeds over the entire domain (unpublished data). Therefore, the apparent additional constraint is related to the microtubule growth and/or shrinkage ($V_{growth} = 0.16$ μm/s; $V_{shrink} = -0.25$ μm/s). Indeed, a prerequisite for S_2 is that motor complexes actually reach the ends of growing microtubules. This is only possible if the plus end–directed motor is faster than the growth speed of the filaments ($u > V_{growth}$). Furthermore, to be able to pull a microtubule by its plus end toward the center of the other aster (Fig. 3, S_2), the minus end–directed motor should also be faster than the growth speed ($|v| > V_{growth}$). Because these conditions apply on the effective speed at which motors move, which is usually only a fraction of V_{max}, the slowest speed found for S_2 is not V_{growth}, but a somewhat higher value, ~0.25 μm/s. Further screening should produce a limit closer to V_{growth}.

Screen 3c

A heteromotor complex screen in which the motors could stay attached even to shrinking microtubules was performed ($P_{end} = P_{end\_growing} = P_{end\_shrinking}$ between 0.04 s^{-1} and 50 s^{-1}). With this, a plus end–directed motor who has reached the plus end of a shrinking microtubule would remain attached, following the end toward the center of the aster. The solutions S_2 are now over all the region $u \times v < 0$ and $u + v > 0$ (Fig. 6), meaning that the additional constraints on the motor speeds were released by allowing them to hold on shrinking microtubule ends.

The difference between S_1 and S_2 is revealed by looking directly at the forces; in S_2, motor complexes attached to the region of antiparallel microtubule overlap are pushing, whereas in S_1, they are pulling (Fig. 3). S_3 and S_4 are quite similar to S_1, and a portion of the forces in S_3 or S_4 are always due to S_1 contributions. They are not described here in detail, but can be understood from Fig. 3, and examples of simulations can be found online (http://www.embl-heidelberg.de/ExternalInfo/nedelec/asters). Last, we examined the distance between the asters in the solutions S_1 and S_2. Fig. 3 shows that in 1D, with static microtubules, the center to center distance in the full antiparallel overlap S_1 is mostly determined by the length of the microtubules. Simulations with dynamic microtubules are more complex, but can be compared because they all include microtubules following the same dynamic, which have on average the same length of ~7 μm. The examples in Fig. 2 (top) have aster–aster distances of 7.4 ± 1 μm, 8.2 ± 0.24 μm, and 13.9 ± 1.1 μm, respectively, from left to right (average and standard devia-

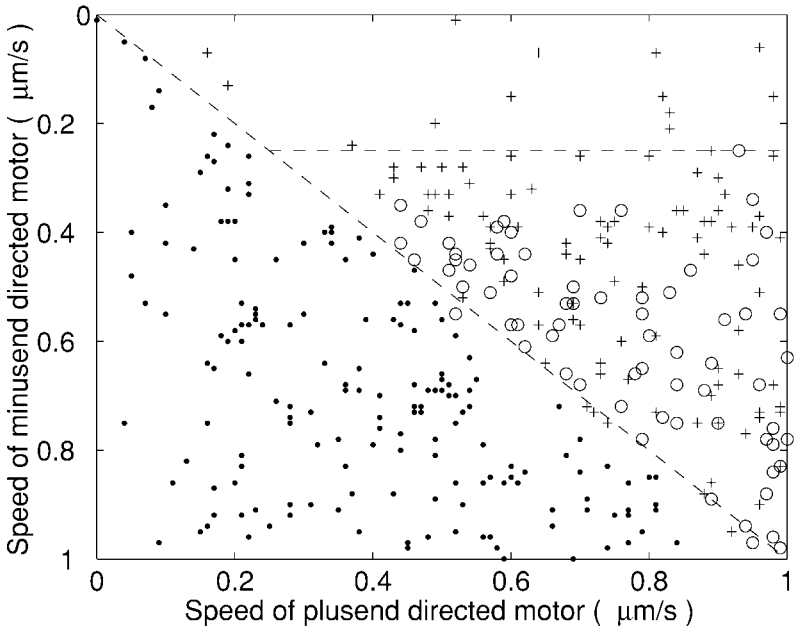

Figure 6. **Probing the constraints on the speeds.** Each symbol represents one simulation and is plotted here as a function of the unloaded speeds (V_{max}) of the two motors in the complex. Dots, S_1 produced in screen 3a; circles, S_2 produced in screen 3b, in which the motor could stay attached only to growing microtubules; pluses, S_2 produced in screen 3c when the motor could stay attached also to shrinking ends.

tions from 100 simulations), although they all realize the same equilibrium S_1. Hence the characteristics of the motors and microtubules contribute together to the equilibrium. Overall averages show that asters in a partial antiparallel overlap S_2 are 11.4 ± 4.2 µm apart, whereas they are distant by 9.3 ± 3.9 µm in a full antiparallel overlap S_1. Asters are further apart in S_2 than in S_1, but the two distributions largely overlap; consequently with dynamic microtubules, S_1 and S_2 are not as easily distinguishable from the aster to aster distance as Fig. 3 might suggest.

Discussion

Recent progress in light microscope technology has revealed the dynamic nature of biological organization. Many structures in the cell are in fact self-organized steady-state assemblies resulting from continuous stochastic interactions at the molecular level. To describe and understand these structures in quantitative terms, there is a need for new tools allowing the analysis of the collective behavior of molecules. The mitotic spindle is a good example of a self-organizing cellular structure, whose function is to segregate chromosomes into the newly forming daughter cells. Spindle morphologies can vary considerably amongst different cell types; for example, some spindles have well-focused poles, whereas others do not. Or some pull on the chromosomes using an antiparallel microtubule overlap to counterbalance the forces, whereas others do so by attaching to the cell cortex. The spindle is host to many interesting phenomena, e.g., the dynamic instability of microtubules, the local stabilization of microtubules by chromatin and by MAPs, or the action of various molecular motors. Integrating all these to explain the different spindle morphologies will most certainly require the use of computer simulations. Here I have modestly started to integrate some simple properties into a simulation and I used it to study a single feature known to occur in spindles: microtubules originating from opposite poles can form stable antiparallel overlaps. As a starting point, one can do this while ignoring many other aspects of spindle assembly by artificially reducing the spindle to two asters of microtubules, with which the feature is first tested. It is still unknown if motors alone can produce stable antiparallel interactions. This question was addressed here theoretically, ignoring for example that force production by microtubule assembly/disassembly might be necessary to achieve this feature.

The systematic computer screening shows that heterocomplexes of plus and minus end–directed motors can produce stable interaction patterns between microtubule asters. These figures resemble spindles because they have similar features: two poles and overlapping antiparallel microtubules between them. On the contrary, the various mixtures of homocomplexes computed only led to fusion or full separation of the two asters. The failure to find stable antiparallel overlaps with homocomplexes could be attributed to limitations of the screen, e.g., the number of simulations was too small, but there might be more fundamental reasons. First, homocomplexes acting on just two microtubules do not produce antiparallel overlap but instead organize them into a parallel configuration (Fig. 7). Second, in the simple situation studied, a partial overlap in which both pulling and pushing forces are proportional to the amount of microtubule overlap is bound to be unstable.

The screens were computed in 1D and 2D with similar results (unpublished data), and the solutions also exist in 3D (http://www.embl-heidelberg.de/ExternalInfo/nedelec/asters). The solutions $S_{1–4}$ could uphold static (unpublished data) or dynamic microtubules, with some differences in their requirements on the motors, as was shown for S_2. Because the simulations are based on discrete stochastic events, the solutions can also tolerate some variation in the parameters that define these events: e.g., binding rates, unbinding rates, and the number of motors (http://www.embl-heidelberg.de/ExternalInfo/nedelec/asters). The different solutions show us simple ways in which a balance of forces can reliably be achieved (Fig. 3). Importantly, the simulations showed that all these situations are stable: if the microtubules disas-

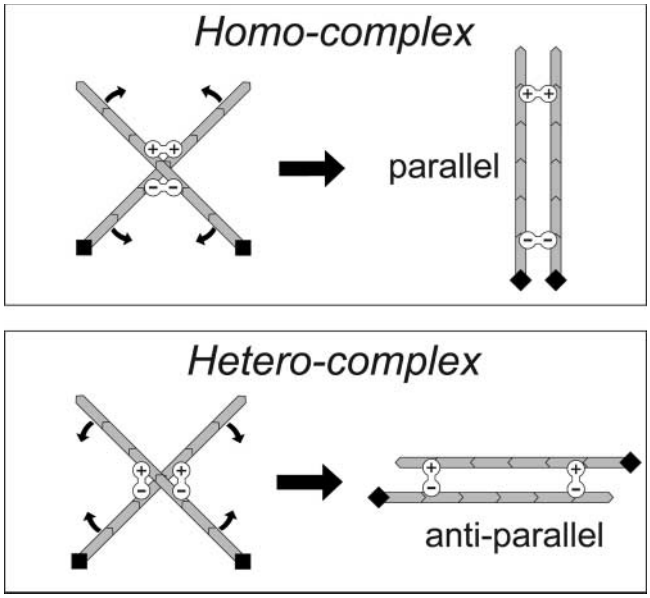

Figure 7. **The zipper effect.** Schematically, the action of homocomplexes on two microtubules produces parallel microtubule overlap, whereas heterocomplexes produce antiparallel overlaps.

semble, or if by chance the asters are displaced too far, the forces will be modified, and the asters will be dragged back together. The reverse is true when the microtubules grow or if the asters get too close. The mechanical stability of the equilibrium is a simple but essential property realized in each solution. Surprisingly, the simulations suggest that the solutions are unique stable equilibria, which can be reached from any initial configuration, and this makes them quite interesting from a cell biological point of view.

The simulation was initially developed to study an in vitro mixture of pure proteins, and its first validation came from comparison with experiments (Nédélec and Surrey, 2001; Surrey et al., 2001). The model for the motors is inspired from the measured behavior of kinesin, which is a processive motor whose speed varies almost linearly with the load (Hunt et al., 1994; Svoboda and Block, 1994). This is not intended to be realistic in every detail, but could represent other processive motors or regulated processive assemblies of nonprocessive motors. However, a limitation is that the model might not correspond to isolated nonprocessive motors.

Inside the cell, many effects could allow more elaborate types of equilibria. For example, microtubules can produce forces without motors (Holy et al., 1997), and some motors might influence microtubule stability (Hunter and Wordeman, 2000). Mechanisms of biological regulation or the presence of chromosomes could change the composition or properties of some molecules in time or space, or as a feedback of the present organization. Some key elements of the spindle, such as the proposed "matrix" (Kapoor and Mitchison, 2001), might still be missing. Clearly, cells have many other ways to realize a stable balance of force. Yet, the solutions described in this paper are simple and emerge from core properties of microtubules and motors. They represent conceptual solutions that could be generated in vivo by various molecular mechanisms.

The solutions point to two interesting possibilities that can be tested. The first one is that a pause of the motors at microtubule ends gives them additional morphogenetic properties, confirming previous proposals (Hyman and Karsenti, 1996; Kruse and Julicher, 2000; Nédélec and Surrey, 2001). The second, and new, possibility is that heterocomplexes with both plus and minus end–directed motor activities have the capacity to produce antiparallel overlaps, from which stable interactions can be made. Such complexes could easily be built in the cell. This might not necessarily be by direct and stable interactions between different motor proteins, but rather by transient association, allowing its regulation both in space and time during mitosis. There is some evidence for interaction between motors of opposite directionality (Blangy et al., 1997), but, to my knowledge, direct physical association between motors of opposite polarity in vivo has not been proven so far. It is worth pointing out that in the spindle of some organisms, there is a microtubule flux toward the poles (Waterman-Storer and Salmon, 1997). In the model, this flux would be integrated in first approximation by subtracting the flux speed from the speed of all motors. The putative plus and minus end–directed motor complexes could be built from the association of a static microtubule binding protein with a plus end–directed motor, which would need to be faster than the microtubule flux. In this situation, one can even imagine that two plus end–directed motors of very different speeds would make an effective plus–minus complex.

In summary, computer simulations have been described and used to systematically explore how a stable balance of forces can be achieved between two asters and soluble motor complexes. Four solutions were found (Fig. 3) that achieve stable equilibrium by combining simple properties of polar filaments and directed motors. The different qualitative requirements on the motors for each of these solutions were expressed simply and should be testable experimentally. All the solutions rely ultimately on a common "frustration" principle: by their movement, the heterocomplexes place the motors on the opposite side from where they would naturally go; a minus end–directed motor near the plus ends of a microtubule, or vice versa. With this simple rule, we can already imagine other solutions. For example any mechanism that leads to the localization of a plus end–directed motor to the center of asters or a minus end–directed one near the plus ends of microtubules, while leaving the motor free to grab passing microtubules, can also lead to stable interactions between asters.

Materials and methods

Animations, executables, and instructions can be found online at http://www.embl-heidelberg.de/ExternalInfo/nedelec/asters. Requests for the source code should be sent to the author or to EMBL Enterprise Management Technology Transfer.

The principle of the simulation, simulated dynamics, is intuitive: from an initial configuration, the future of the sample is calculated in small successive time steps. All the forces and movements of individual filaments and motors are calculated by solving the equations of motion, which are set according to the laws of classical mechanics. These motions include simple and natural processes; the filaments diffuse, grow and shrink, and respond elastically to deformation. The motors diffuse, can bind and move onto the filaments, exert forces on them, and eventually unbind. All inter-

actions are based on "first principles." All parameters could, in principle, be directly obtained from single molecule experiments. Importantly, this makes the conditions we find on parameter values simple to interpret. Because the thermal noise present in the world of molecules is essential to their function, the simulation is largely stochastic. The probabilities of most events (e.g., binding and release of motors) are calibrated according to rates given as parameters to the program, but their exact timing is not predictable. The simulations thus include at least some of the noise present in nature.

All features of the natural world cannot, and should not, be retained. Among the many simplifications introduced, the biggest is that two filaments will only feel their respective presence if they are somehow linked by motors. As a consequence, the filaments can cross or overlap freely without any steric or hydrodynamic interactions. In some of the simulations that we discarded (fusion and oscillatory solutions), the distance between the asters came close to zero. The solutions S_{1-4}, on the contrary, were selected because the distance between the asters was always >2 μm, and steric interaction should not alter them significantly. With the methods described, a PC build in 2001 could each day simulate a fully connected structure of 1,000 microtubules. Such a system is roughly comparable in size to an animal mitotic spindle. Hence, the limitations are not so much numerical, but really in the intrinsic biological complexity of the subject.

For each time step, the objects in the system are considered in random order in each of the following: (a) dynamic instability of microtubules (stochastic transitions between growing/shrinking state, lengthen/shorten according to state); (b) solve the motion of the filaments, considering their elasticity, the action of motor complexes, and Brownian forces; (c) stochastic attachment of free motors, detachments of bound ones, optional detachment if the force is above a threshold, and displacement along the filament; and (d) diffusion of free motor complexes. These processes are detailed below.

Microtubules

Simulated microtubules are linear, infinitely thin, oriented objects that mechanically behave like inextensible elastic rods (Feynman, 1989). The position of a microtubule is represented by $N + 1$ points M_i, for $i = 0$ to N, with all the distances $|M_iM_{i+1}|$ being equal. M_0 is the minus end and M_N is the plus end. The length L of the microtubule can take any value, and as it grows or shrinks, points are dynamically added or removed to ensure that at all times N achieves the minimum of the absolute value of $R - L/N$ while staying ≥ 1. R is a parameter of the model called the filament section length. Hence, all segments $|M_iM_{i+1}|$ on the same microtubule have the same length L/N, which is always close to R, but L/N can vary from microtubule to microtubule.

Smaller values of R ensure more accurate computation, but require more processor time. One consideration when choosing R is that it should be smaller than the radius of curvature of the filaments, and this can be checked after the simulation has been performed. The force needed to fold a filament on a radius of curvature R is $\sim E/R^2$, where E is its mechanical bending modulus. Knowing the motor's maximum forces, this formula provides a guideline to initially choose R. The simulations presented here were calculated with $R = 1.2$ μm ($E/R^2 \approx 14$ pN), and occasionally $R = 0.5$ μm.

Simulated microtubules are not stretchable, but can bend elastically under external forces or Brownian motion. For any three consecutive points M_{i-1}, M_i, and M_{i+1}, the program calculates $F = E \times (N/L)^3 \times (M_{i+1} - 2M_i + M_{i-1})$, where E is the bending modulus (20 pN μm^2 for microtubules; Kurachi et al., 1995) and L/N the distance between consecutive points. The force 2F is applied to M_i, while $-F$ is applied to M_{i-1} and M_{i+1}. This linear elastic torque realizes the theoretical value (Feynman, 1989) under small deformations.

Asters

An aster is a set of microtubules attached at their minus end with static and permanent Hookean links. Its structural integrity is independent of the activity of the motors. The microtubules are also attached laterally to their side neighbors at some distance from the center (0.75 μm). In 3D, the aster is built similarly, by using a triangulation of the isocahedron as a template. The resulting structure is always a very rigid tensegrity construction, in which the microtubules are regularly distributed. Asters move or rotate as a whole without much stretch (typically <2 nm) in their static links.

Dynamic instability

The microtubule's dynamic instability is modeled according to experimental data obtained for centrosome-nucleated asters in mitotic *Xenopus* egg extract (Dogterom et al., 1996). The minus end of the microtubule, in the center of the aster, is static. The plus end is either shrinking or growing, and the transitions between these two states depend only on the microtubule length L (Dogterom et al., 1996), making longer microtubules less stable: catastrophe frequency (s^{-1}) is equal to $L \times 0.003$, and rescue frequency (s^{-1}) is $(13 - L) \times 0.00333$ (when L is in μm). The growth and shrinkage speeds are constant, $+10$ and -15 μm/min, respectively. For simplicity, microtubules do not shrink below 1 μm, hence their number is constant. The microtubules have, under these conditions, a mean length of ~ 7 μm, with a (large) standard deviation of ~ 3 μm. They spend $\sim 54\%$ of their time growing, $\sim 31\%$ of their time shrinking, and $\sim 15\%$ of their time at their minimal length, 1 μm, waiting for a rescue.

Simpler models, where the transition probabilities are independent of the microtubule length, can also be used. In fact, the simulations were initially performed with static microtubules of fixed length and produced very similar results to those presented here (unpublished data). Dynamic instability is considered here, because sudden catastrophes and fast microtubule disassembly make the asters very variable and, hence, unpredictable structures. Consequently, the simulations demonstrate better that the solutions are very stable with respect to the number of microtubules and their lengths.

Motors

The minimal processive entity that can bind to a microtubule and move on its surface is called a "hand." A hand is always associated with a second one, forming a bifunctional soluble motor complex.

Hands

Each hand (a single motor) is either detached or attached to a microtubule, and transitions between these two states occur in the following way. A free hand is at a position defined by the complex it belongs to. From this position, it may bind, with given rate P_{on} (s^{-1}), on every microtubule geometrically closer than a given parameter ϵ (μm), the reach of the motor. When ϵ is small, binding is limited by diffusion (Nédélec et al., 2001). Bound hands are entirely characterized by a record of the microtubule they are attached to and the position (or abscissa) at which they are bound, counted from the minus end. Bound motors detach stochastically with a rate P_{off} (s^{-1}), but otherwise move along the microtubule in a direction defined by the intrinsic directionality of the motor. A bound motor that has, by its movement, reached the end of a microtubule detaches with a different unbinding rate P_{end} (s^{-1}). We can imagine that P_{off} is a property of a moving motor, which goes through rounds of ATP hydrolysis, whereas P_{end} is a property of an immobile motor probably arrested in one configuration at the end of its track. Both rates can therefore have unrelated values.

Stochasticity

All the discrete events in the simulation, binding and unbinding events, catastrophes, and rescues, are modeled stochastically. To decide if a possible event with a rate P (s^{-1}) should be performed or not during a period dt (10^{-2} s), the program draws a pseudorandom number (x) between 0 and 1 (Matsumoto and Nishimura, 1998). The event is performed if $x < P \times dt$. Practically, this procedure limits the rates to $P < 50\ s^{-1}$ (0.5/dt). Rates $>100\ s^{-1}$ are equivalent and result in an immediate and thus nonstochastic action.

Unbinding from the microtubule ends

The detachment of a motor from the plus end of a microtubule could be different whether this end is shrinking or growing. In all generality, there are two rates, $P_{end\_shrinking}$ and $P_{end\_growing}$. For clarity, the exploration is limited to three situations: (1) screens 1, 2, and 3a, motors always detach at all ends ($P_{end\_shrinking}$ and $P_{end\_growing}$ both $>100\ s^{-1}$, i.e., immediate); (2) screen 3b, motors detach fast from shrinking ends and slowly from growing ends ($P_{end\_shrinking}$ immediate and $P_{end} = P_{end\_growing}$ randomly taken within 0.04 and 50 s^{-1}); and (3) screen 3c, motors detach equally from shrinking and growing ends ($P_{end} = P_{end\_shrinking} = P_{end\_growing}$ randomly taken within 0.04 and 50 s^{-1}). The minus ends of the microtubules are not static, and minus end–directed motors always unbind from this end with the same rate, P_{end}.

Motor movement

All interactions between motors while bound to the same microtubule are neglected. Motors pass or cross each other without interacting. Similarly, the microtubule lattice never saturates, and more motors can always bind. This simplification should be true at low density of motors, but might break down at high densities. Simulated microtubules are "smooth" and their structure is neglected; they also have similar properties all along their length and are all equivalent. Motors always bind to the geometrically closest point on the microtubule, and not to specific sites that would be defined by the tubulin lattice. Similarly, if a motor moves at speed V, its abscissa will be simply increased during a time dt by $V \times dt$, whether or not this represents a multiple of the tubulin lattice. An unloaded motor is

moving at a speed given by a parameter V_{max}, plus end directed if $V_{max} > 0$ or minus end directed if $V_{max} < 0$. We will see later how the effective speed V of the motor is determined by the possible load applied to the motor, created when the motor is part of a complex linking two microtubules.

Motor complexes

A motor complex is a set of two hands linked by a Hooke's spring (i.e., a linear force). These two hands behave independently, with the exception that a complex cannot be bound twice to the same or to successive segments on the same microtubule. The states of its two hands determine the state of the complex and its behavior. Free complexes diffuse with a coefficient D (20 $\mu m^2/s$). Complexes attached to only one microtubule are transported along this microtubule at the unloaded speed of the attached hand without exerting force. On the contrary, a complex attached to two microtubules effectively links them with a force $F = K \times dx$, which is proportional to the separation vector between the two hands, dx. For simplicity, the stiffness K (pN/μm) is the same for all complexes.

Force–velocity relationship

Four similar models for the force–velocity curves of hands were used, which are defined by two parameters: a maximum force, F_{max} (always positive), and a maximum speed, V_{max}. Movement occurs at decreasing speed for increasing load; the simplest model implements a full linear force–velocity dependency, $V = V_{max}(1 - F_{axis}/F_{max})$, where the scalar F_{axis} is the projection of the force F on the axis of the microtubule, taking into account the directionality of the motor. $F_{axis} > 0$ for a force that resists the natural movement of the motor, and $F_{axis} < 0$ for a force that helps it. With this simple model, a motor pulling a passive load, for example a bead, would never exceed its maximum force (F_{max}) or its maximum velocity (V_{max}). However, this motor can be forced backward, for example if it is pulled by other motors.

In experiments, a motor like kinesin has never been observed to make a backward step. The model therefore includes two mechanisms to prevent backward motions. The first limits the linear range to $-F_{max} < F_{axis} < F_{max}$. Outside this range, the motor is either moving at $2V_{max}$ or held immobile, respectively. The second mechanism imposes detachment on motors if they satisfy $F^2 > \dim F_{max}^2$. The test is here on the norm of the vector force F, hence the factor dim (the number of dimensions in space), to allow a motor to effectively reach a stall force along the filament axis, with an additional off-axis component. Three models for the motors are derived from the full linear one by including one or both of these restricting mechanisms. However, apart from oscillations, there is no strong qualitative difference between all four models in the present study. The oscillations required that the detachment of a motor depends on its load, which is only achieved here in the models that include detachment at maximum force ($F^2 > \dim F_{max}^2$).

Elasticity of the motors

We can generally expect that molecules act as nonHookean springs with a nonzero resting length. For simplicity, the simulated complexes follow Hooke's law with a null resting length (kinesin stiffness seems to be constant, ~400 pN/μm; Kawaguchi and Ishiwata, 2001). This contributes greatly to the simplicity and to the numerical stability of the final algorithm, but implies that the stiffness (K), the stalling force (F_{max}), and the reach (ϵ) depend on each other.

1. The equipartition theorem of statistical mechanics states that at a temperature T, any spring stores on average an energy $\dim/2 k_B T$ (this is also true in the simulations). If the stiffness of the spring is K, this corresponds to a random force of magnitude $<F^2> = \dim \times K \times k_B T$. For the motors that detach at their maximum force, this random force should be $<F_{max}$. Therefore, to simulate kinesin (F_{max} = 5 pN), K as high as 500 pN/μm is appropriate, but to simulate a weaker motor with a stalling force of 0.5 pN, the stiffness needs to be lower, for example K = 5 pN/μm.

2. Consistency of the model also requires that the force at the time of binding be inferior to the maximum force of the motor, i.e., $K \times \epsilon < F_{max}$.

For the screen presented here, K and F_{max} were drawn randomly between 5 and 60 pN/μm and 0.5 to 2 pN, respectively. To satisfy the first condition with a safety factor of 3, only sets which satisfied $\dim \times K \times k_B T < 1/9\ F_{max}^2$ were kept. To satisfy the second condition, ϵ was always equal to F_{max}/K and altogether varied between 25 and 200 nm.

Linearity of the forces

A position (X) on a microtubule between two consecutive points M_i and M_{i+1} is calculated as $X = M_i + (M_{i+1} - M_i)|M_iX|/|M_iM_{i+1}|$. The force exerted by a complex is the difference of two such positions, $F = K(Y - X)$. F is acting on the first microtubule at the position X, and $-F$ applies to the second microtubule at point Y. For the first microtubule, F is further split, according to the position of X between M_i and M_{i+1}: $F_i = F|XM_{i+1}|/|M_iM_{i+1}|$ applies in M_i, and $F_{i+1} = F|M_iX|/|M_iM_{i+1}|$ applies in M_{i+1}. Hence, the contribution of a motor link is linear.

Initialization and confinement inside a box

Motors are initially free and uniformly distributed over the simulation box of 60 × 60 μm. Confinement is achieved by reflecting boundaries. To ensure that the asters are close enough to interact, they are set randomly within the 12 × 12-μm central square. The microtubules are all initially 1 μm long, in a growing state, but lose this synchrony after ~100 s. Confining the filaments was not necessary, as the box is much larger than their size.

Movement of the filaments

As usual on the scales of micrometers, the movement is dominated by viscosity and inertia is neglected (Berg, 1993). The speed of each microtubule point is proportional to the sum of the forces acting on it: $dM_i/dt = mob_i \times F_i$. The mobility mob_i of the N + 1 points in a microtubule of length L is the same for all i: $mob_i = H(N+1)(4\pi \text{ viscosity } L)^{-1}$. For simplicity, no correction is made for the filament orientation or for hydrodynamic interactions. To yield more accurate drag forces, the factor $H = \log_e(2\ \mu m/25\ nm) = 4.38$ corrects for the tubular shape of the microtubule (Hunt et al., 1994). It is based on a hydrodynamic cut-off length of 2 μm and the diameter of the microtubules, 25 nm. All the simulations are performed with a viscosity of 0.05 pN s/μm^2, or ~50 times the viscosity of water, and are intended to represent the conditions inside a cell or a developing egg, of which the viscosity could be as high as 100 times the viscosity of water (Hiramoto, 1970).

Integration of the motion

Altogether, the model reduces to the points defining the microtubule's positions, connected by forces that are linear in the coordinates of these points (elasticity, motor complexes, and aster static links). The problem is technically difficult because the total number of variables is large (typically 2,000 for the current work). The first order differential equation is solved implicitly with a constant time step $dt = 10^{-2}$ s. Practically, the coordinates of the points M_i of all microtubules at time t are pooled in a vector (M^t). Scanning through the interactions builds a matrix (A) such that $A \times M^t$ is the force acting at time t on the points. To represent the Brownian forces in the system, a random vector (E) is calibrated to yield $<E_i^2> = k_B T/(mob_{avg} \times dt)$, with $mob_{avg} = H(4\pi \text{ viscosity } R)^{-1}$, and $k_B T$ for a temperature of 37°C. The Jacobian projection (P) defined by the conservation of the lengths M_iM_{i+1} for each microtubule is calculated. Finally, the implicit system $M^{t+dt} - M^t = dt\ mob \times P(A \times M^{t+dt} + E)$ is solved to get M^{t+dt}, with mob the diagonal of all the mob_i. The constraints are not perfectly preserved, and the points are further moved to restore the length of each microtubule. This is only a small contribution to the movement of the points, usually <0.1 nm per time step and per point (the diffusion is ~40 nm/step). This correction is done while conserving the barycenter of each microtubule to avoid introducing any systematic error. The most intensive part of the computation is usually to solve the linear system, and processor times vary mostly with the size of the matrix, i.e., the number of microtubules considered. The simulations took here on average ~20 min in 1D, ~3 h in 2D, and ~5 h in 3D on a 700-MHz Pentium III Linux PC.

Internal controls

To check that the choice of time step (dt), section length (R), and size of the box did not affect the outcome of the simulations beyond numerical precision, simulations were repeated with all possible combinations of R = 0.5 or 1 μm and dt = 5 or 10 ms within a simulation box of 60 or 120 μm, while conserving the concentration of the motor complexes. All these different choices produced virtually identical outcomes (http://www.embl-heidelberg.de/ExternalInfo/nedelec/asters). Indeed, the numerical precision achieved by the standard choice of R, dt, and box size is sufficient with respect to the Brownian forces in the model.

Parameter values

Appropriate values for kinesin would be roughly $F_{max} \approx 5$ pN, $V_{max} \approx 0.8$ μm/s, K ≈ 100 pN/μm, $\epsilon \approx 50$ nm, $P_{on} \approx 50$ /s, and $P_{off} \approx 1$ /s. These estimates are used as guidelines to set the ranges in which the values of the motor parameters are drawn randomly for any individual simulation (Table 1). The number of motors in the simulation is also chosen randomly, their force–velocity relation is any one of the four described. The number of microtubules in the aster is chosen between 20 and 80, as this is typically the number of microtubules nucleated by a centrosome in *Xenopus* egg extracts. In the 1,000 s simulated, very slow motors would not have enough time to produce a stable situation between the asters. In the automatic

screen, these slowly evolving interactions would be mistakenly selected, because they persist during the simulated period. To limit this, I a priori did not consider simulations in which the speeds of the motors were below 0.01 μm/s, or for which rates were below 0.04/s.

I thank Eric Karsenti and Thomas Surrey (European Molecular Biology Laboratory [EMBL]) for their precious input in this work, their daily support, and our discussions. I also thank Stephanie Blandin, Damian Brunner, Michael Knopp, Oleg Lerner, Iain Mattaj (EMBL), Marileen Dogterom (AMOLF, Amsterdam, Netherlands), Stan Leibler (Rockefeller University, New York, NY), A.C. Maggs (ESPCI, Paris, France), and Jean-Claude Nédélec (École Polytechnique, Palaiseau, France).

Submitted: 12 February 2002
Revised: 30 July 2002
Accepted: 30 July 2002

References

Berg, H. 1993. Random Walks in Biology. Princeton University Press, Princeton, NJ.

Bayley, P.M., M.J. Schilstra, and S.R. Martin. 1989. A simple formulation of microtubule dynamics: quantitative implications of the dynamic instability of microtubule populations in vivo and in vitro. *J. Cell Sci.* 93(Pt. 2):241–254.

Blangy, A., L. Arnaud, and E.A. Nigg. 1997. Phosphorylation by p34 protein kinase regulates binding of the kinesin-related motor HsEg5 to the dynactin subunit p150. *J. Biol. Chem.* 272:19418–19424.

Bourdieu, L., T. Duke, M.B. Elowitz, D.A. Winkelmann, S. Leibler, and A. Libchaber. 1995. Spiral defects in motility assays: a measure of motor protein force. *Phys. Rev. Lett.* 75:176–179.

Dogterom, M., A.C. Maggs, and S. Leibler. 1995. Diffusion and formation of microtubule asters: physical processes versus biochemical regulation. *Proc. Natl. Acad. Sci. USA.* 92:6683–6688.

Dogterom, M., M.A. Felix, C.C. Guet, and S. Leibler. 1996. Influence of M-phase chromatin on the anisotropy of microtubule asters. *J. Cell Biol.* 133:125–140.

Feynman, R. 1989. Elasticity. *In* The Feynman Lectures on Physics. Vol. 2. Addison Wesley, Reading, MA.

Gibbons, F.D., J.F. Chauwin, M. Desposito, and J.V. José. 2001. A dynamical model of kinesin-microtubule motility assays. *Biophys. J.* 80:2515–2526.

Gliksman, N.R., R.V. Skibbens, and E.D. Salmon. 1993. How the transition frequencies of microtubule dynamic instability (nucleation, catastrophe, and rescue) regulate microtubule dynamics in interphase and mitosis: analysis using a Monte Carlo computer simulation. *Mol. Biol. Cell.* 4:1035–1050.

Hiramoto, Y. 1970. Rheological properties of sea urchin eggs. *Biorheology.* 6:201–234.

Holy, T., M. Dogterom, B. Yurke, and S. Leibler. 1997. Assembly and positioning of microtubule asters in microfabricated chambers. *Proc. Natl. Acad. Sci. USA.* 94:6228–6231.

Hunt, A.J., F. Gittes, and J. Howard. 1994. The force exerted by a single kinesin molecule against a viscous load. *Biophys. J.* 67:766–781.

Hunter, A.W., and L. Wordeman. 2000. How motor proteins influence microtubule polymerization dynamics. *J. Cell Sci.* 113(Pt. 24):4379–4389.

Hyman, A.A., and E. Karsenti. 1996. Morphogenetic properties of microtubules and mitotic spindle assembly. *Cell.* 84:401–410.

Kapoor, T.M., and T.J. Mitchison. 2001. Eg5 is static in bipolar spindles relative to tubulin: evidence for a static spindle matrix. *J. Cell Biol.* 154:1125–1133.

Karabay, A., and R.A. Walker. 1999. Identification of microtubule binding sites in the ncd tail domain. *Biochemistry.* 38:1838–1849.

Karsenti, E., and I. Vernos. 2001. The mitotic spindle: a self-made machine. *Science.* 294:543–547.

Kashina, A.S., R.J. Baskin, D.G. Cole, K.P. Wedaman, W.M. Saxton, and J.M. Scholey. 1996. A bipolar kinesin. *Nature.* 379:270–272.

Kawaguchi, K., and S. Ishiwata. 2001. Nucleotide-dependent single- to double-headed binding of kinesin. *Science.* 291:667–669.

Kruse, K., and F. Julicher. 2000. Actively contracting bundles of polar filaments. *Phys. Rev. Lett.* 85:1778–1781.

Kurachi, M., M. Hoshi, and H. Tashiro. 1995. Buckling of a single microtubule by optical trapping forces: direct measurement of microtubule rigidity. *Cell Motil. Cytoskeleton.* 30:221–228.

Matsumoto, M., and T. Nishimura. 1998. Mersenne Twister: a 623-dimensionally equidistributed uniform pseudo-random number generator. *ACM Transactions on Modeling and Computer Simulation.* 8:3–30.

McDonald, H.B., R.J. Stewart, and L.S. Goldstein. 1990. The kinesin-like ncd protein of *Drosophila* is a minus end-directed microtubule motor. *Cell.* 63: 1159–1165.

Nakazawa, H., and K. Sekimoto. 1996. Polarity sorting in a bundle of actin filaments by two-headed myosins. *J. Physiol. Soc. Japan.* 65:2404–2407.

Nédélec, F., and T. Surrey. 2001. Dynamics of microtubule aster formation by motor complexes. *Comptes Rendus de l'Académie des Sciences Série IV.* 6:841–847.

Nédélec, F., T. Surrey, A.C. Maggs, and S. Leibler. 1997. Self-organization of microtubules and motors. *Nature.* 389:305–308.

Nédélec, F., T. Surrey, and A.C. Maggs. 2001. Dynamic concentration of motors in microtubule arrays. *Phys. Rev. Lett.* 86:3192–3195.

Sharp, D.J., K.R. Yu, J.C. Sisson, W. Sullivan, and J.M. Scholey. 1999. Antagonistic microtubule-sliding motors position mitotic centrosomes in *Drosophila* early embryos. *Nat. Cell Biol.* 1:51–54.

Surrey, T., F. Nédélec, S. Leibler, and E. Karsenti. 2001. Physical properties determining self-organization of motors and microtubules. *Science.* 292:1167–1171.

Svoboda, K., and S.M. Block. 1994. Force and velocity measured for single kinesin molecules. *Cell.* 77:773–784.

Waterman-Storer, C.M., and E.D. Salmon. 1997. Microtubule dynamics: treadmilling comes around again. *Curr. Biol.* 7:R369–R372.

Wittmann, T., A. Hyman, and A. Desai. 2001. The spindle: a dynamic assembly of microtubules and motors. *Nat. Cell Biol.* 3:E28–E34.